10. SYNTHESIS OF SHIPBOARD RESULTS: LEG 110 TRANSECT OF THE NORTHERN BARBADOS RIDGE[1]

Shipboard Scientific Party[2]

ABSTRACT

A décollement zone separating an accretionary prism from underthrust sediments and oceanic crust was penetrated for the first time during Leg 110. Sites cored near the deformation front of the northern Barbados Ridge document an accretionary prism consisting of imbricately thrusted Neogene hemipelagic sediments detached from little-deformed Oligocene to Campanian underthrust sediments by a décollement zone composed of lower Miocene to upper Oligocene scaly radiolarian claystone. Biostratigraphic inversions define thrust faults in the accretionary prism that correlate between sites and are apparent on the seismic reflection data. Two sites, located 12 and 17 km west of the deformation front, indicate continuing deformation of the accreted sediments during their uplift. Deformation features include both large- and small-scale folding and continued thrust faulting with development of stratal disruption and the proliferation of scaly fabrics. These features, resembling fabrics of accretionary complexes exposed on land, have developed in sediments never buried more than 400 m deep and retaining 40% to 50% porosity. A single oceanic reference site, located 6 km east of the deformation front, shows incipient deformation at the stratigraphic level of the décollement and pore-water chemistry anomalies both at the décollement level and in a subjacent permeable sand interval. Pore-water chemistry data from all sites define two fluid realms: one characterized by methane and chloride anomalies and located within and below the décollement zone and a second marked solely by chloride anomalies and occurring within the accretionary prism. The thermogenic methane in fluids within the décollement zone requires that fluid be transported more than 25 km along the shallowly inclined décollement surface, without significant leakage into the overlying accretionary prism. Chloride anomalies along faults and a permeable sand layer in the underthrust sequence may be caused by membrane filtration or perhaps smectite dewatering at depth. Low matrix permeabilities require that fluid flow along faults occur through fractures.

INTRODUCTION

The moderate water depths, relatively thin sedimentary cover, and excellent biostratigraphy of the northern Barbados Ridge area provided the impetus for two scientific drilling cruises to that area (Fig. 1). The principal objective of the cruises was to completely penetrate the toe of the accretionary prism. In 1981, Leg 78A of the Deep Sea Drilling Project first documented biostratigraphic evidence for thrust faulting at the deformation front of an accretionary prism (Biju-Duval, Moore et al., 1984). However, the drilling did not continue through the décollement into the underthrust sedimentary sequence to oceanic basement because the hole collapsed in apparently overpressured, unstable zones within the décollement. The suggestions of high fluid pressures, the good structural control provided by the biostratigraphy, and the availability of high-quality site surveys led to ODP Leg 110. Leg 110 was designed not only to drill through the toe of the accretionary prism but also to address numerous questions regarding the hydrologic evolution of these deforming sediments. The specific objectives of Leg 110 were as follows:

1. To penetrate the accretionary complex and subjacent underthrust sediments into oceanic crust.
2. To define the structural geology and physical properties of the accreted and underthrust sedimentary sequences.
3. To compare the accreted and underthrust sedimentary sequences with a) similar but undeformed materials of the Atlantic abyssal plain and b) deformed rocks of uplifted accretionary complexes, such as those exposed on Barbados Island.
4. To document the dewatering processes, fluid migration pathways, and temperature distribution in sediments of, and adjacent to, the accretionary prism.
5. To drill through the décollement to measure *in-situ* pore-water pressures, temperatures, and permeability and to take pore-water samples from within and outside the fault zones.

Major progress was made in accomplishing these objectives by drilling six sites in a single 23-km-long transect which is located about 1 km north of Sites 541 and 542 of DSDP Leg 78A (Figs. 1 to 3).

[1] Mascle, A., Moore, J. C., et al., 1988. *Proc., Init. Repts. (Pt. A), ODP*, 110: College Station, TX (Ocean Drilling Program).

[2] J. Casey Moore (Co-Chief Scientist), Dept. of Earth Sciences, University of California at Santa Cruz, Santa Cruz, CA 95064; Alain Mascle (Co-Chief Scientist), Institut Français du Pétrole, 1–4 Ave Bois-Preau, B.P. 311, 92506 Rueil Malmaison Cedex, France; Elliott Taylor (Staff Scientist), Ocean Drilling Program, Texas A&M University, College Station, TX 77840; Francis Alvarez, Borehole Research Group, Lamont-Doherty Geological Observatory, Columbia University, Palisades, NY 10964; Patrick Andreieff, BRGM, BP 6009, 45060 Orleans Cedex-2, France; Ross Barnes, Rosario Geoscience Associates, 104 Harbor Lane, Anacortes, WA 98221; Christian Beck, Département des Sciences de la Terre, Université de Lille, 59655 Villeneuve d'Ascq Cedex, France; Jan Behrmann. Institut für Geowissenschaften und Lithosphärenforschung, Universität Giessen, Senckenbergstr. 3, D6300 Giessen, FRG; Gerard Blanc, Laboratoire de Géochimie et Métallogénie U. A. CNRS 196 U.P.M.C., 4 Place Jussieu, 75252 Paris Cedex 05, France; Kevin Brown, Dept. of Geological Sciences, Durham University, South Road, Durham, DH1 3LE, U.K. (current address: Dept. of Earth Sciences, University of California at Santa Cruz, Santa Cruz, CA 95064); Murlene Clark, Dept. of Geology, LSCB 341, University of South Alabama, Mobile, AL 36688; James Dolan, Earth Sciences Board, University of California at Santa Cruz, Santa Cruz, CA 95064; Andrew Fisher, Division of Marine Geology and Geophysics, University of Miami, 4600 Rickenbacker Causeway, Miami, FL 33149; Joris Gieskes, Ocean Research Division A-015, Scripps Institution of Oceanography, La Jolla, CA 92093; Mark Hounslow, Dept. of Geology, Sheffield University, Brook Hill, Sheffield, England S3 7HF; Patrick McLellan, Petro-Canada Resources, PO Box 2844, Calgary, Alberta Canada (current address: Applied Geotechnology Associates, 1-817 3rd Ave. NW, Calgary, Alberta T2N OJ5 Canada); Kate Moran, Atlantic Geoscience Centre, Bedford Institute of Oceanography, Box 1006, Dartmouth, Nova Scotia B2Y 4A2 Canada; Yujiro Ogawa, Dept. of Geology, Faculty of Science, Kyushu University 33, Hakozaki, Fukuoka 812, Japan; Toyosaburo Sakai, Dept. of Geology, Faculty of General Education, Utsunomiya University, 350 Mine-machi, Utsunomiya 321, Japan; Jane Schoonmaker, Hawaii Institute of Geophysics, 2525 Correa Road, Honolulu, HI 96822; Peter J. Vrolijk, Earth Science Board, University of California at Santa Cruz, Santa Cruz, CA 95064; Roy Wilkens, Earth Resources Laboratory, E34-404 Massachusetts Institute of Technology, Cambridge, MA 02139; Colin Williams, Borehole Research Group, Lamont-Doherty Geological Observatory, Columbia University, Palisades, NY 10964.

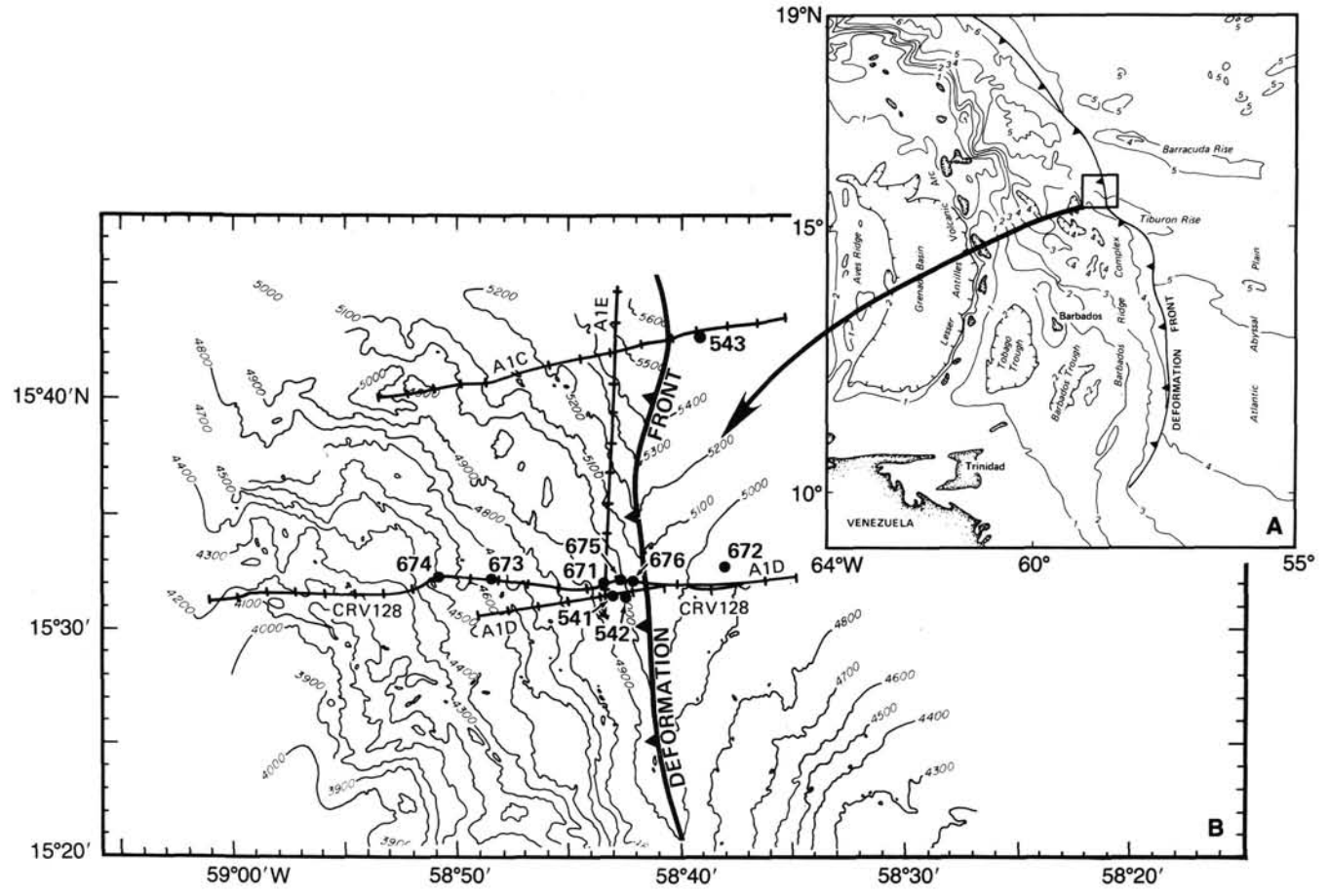

Figure 1. Location map for Leg 110 and Leg 78A drilling sites. Inset shows the regional geography of the Lesser Antilles island arc and Barbados Ridge. Large map shows Seabeam bathymetry and drill sites.

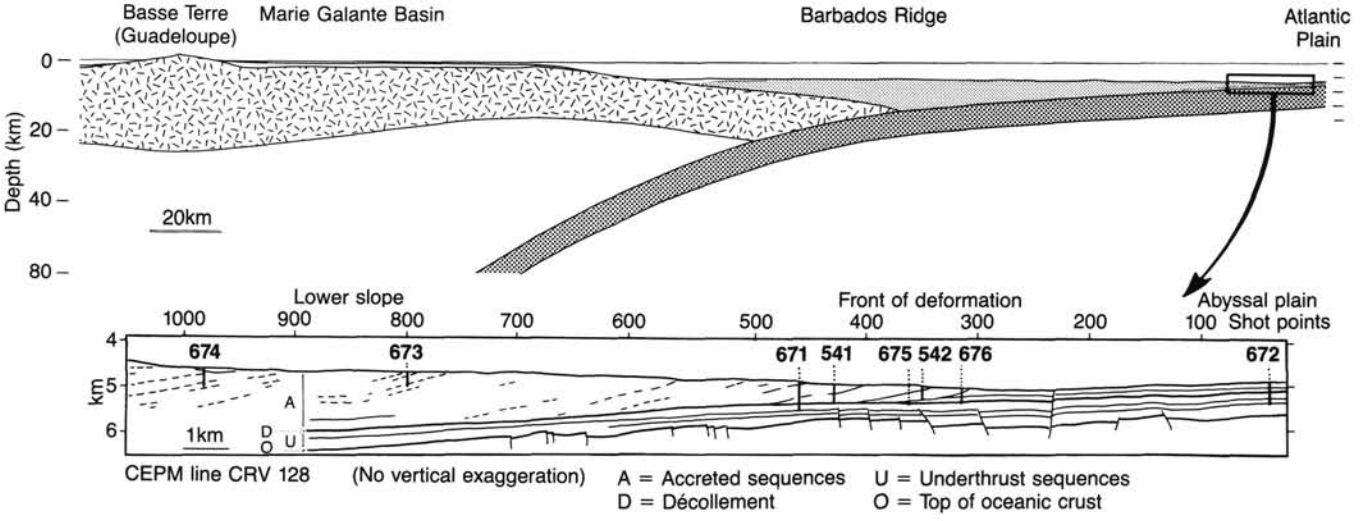

Figure 2. Generalized cross-section of the northern Barbados Ridge and adjacent Lesser Antilles arc. Inset shows depth section generated from seismic line CRV 128 and drilling results.

REGIONAL OVERVIEW

The Lesser Antilles Island Arc (Fig. 1) is the leading edge of the Caribbean Plate, which has been moving eastward with respect to North and South America since at least Eocene time. The resulting subduction of the Mesozoic Atlantic oceanic crust beneath the Caribbean can be traced seismically to a depth of about 200 km (Tomblin, 1975). The most probable plate model suggests that the Atlantic ocean floor underthrusts the Caribbean Plate at 2 cm/yr in a west-southwest direction in the Leg

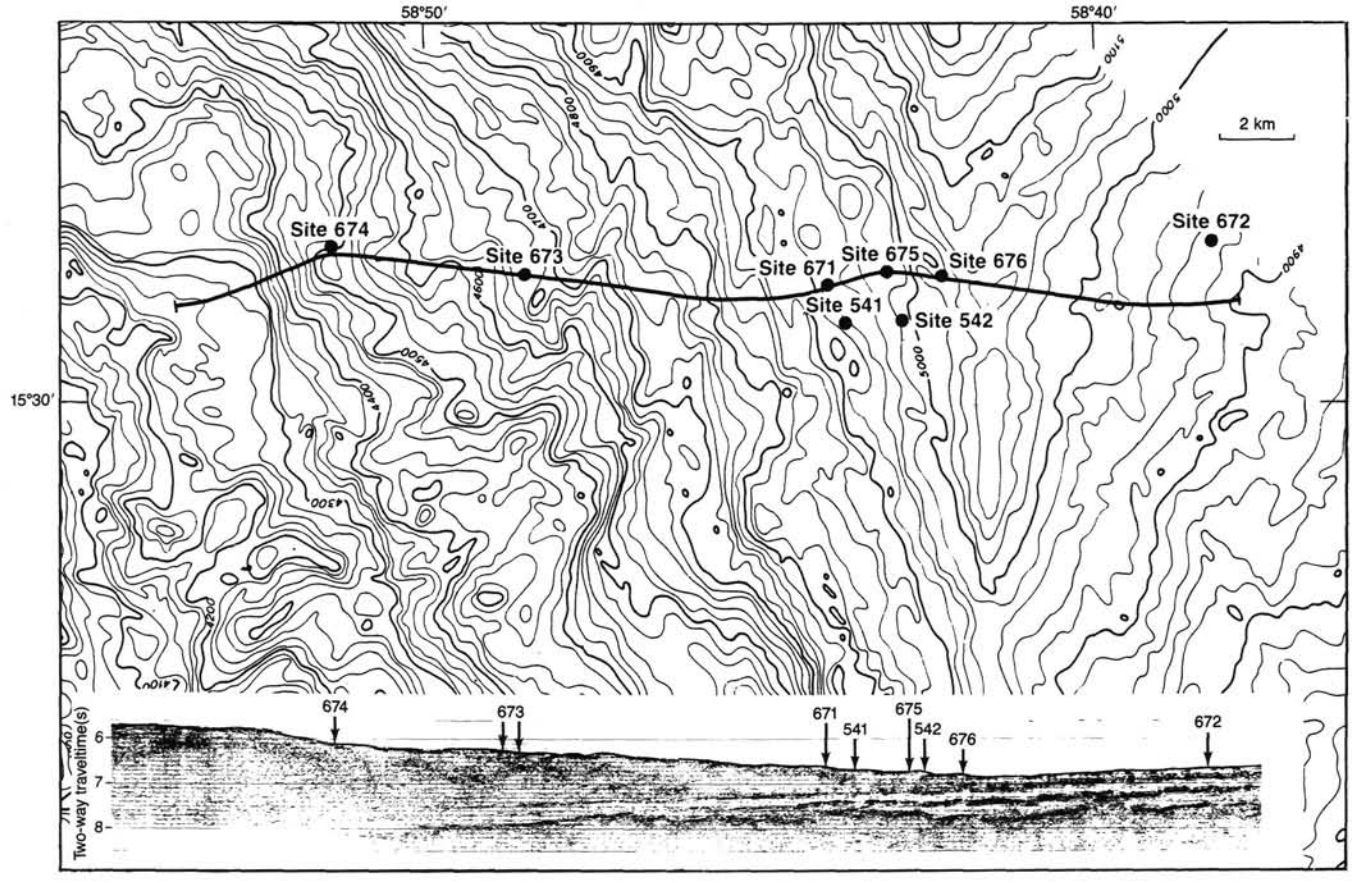

Figure 3. Seabeam bathymetry (m) with site locations and location of seismic line CRV 128 that is displayed at base of figure. Vertical exaggeration of seismic line is 3:1.

110 area (Stein et al., in press) though Sykes et al. (1982) have argued for a higher convergence rate. Seismic slip rates suggest slower underthrusting of about 0.25–0.5 cm/yr (Dorel, 1981; Molnar and Sykes, 1969).

The Lesser Antilles volcanic arc presently includes eight active volcanoes which have erupted magma that varies from basalts to rhyolites (Westercamp, 1977; Tomblin, 1975). The widespread occurrence of Neogene magmatic activity is exposed through the islands (Maury and Westercamp, 1985). Lower Eocene to Oligocene lava flows, pyroclastics, and intrusive rocks are restricted to the northern and southern segments of the arc only. This older volcanic activity reflects the initial underthrusting of Atlantic crust in a subduction zone of the present geometry. Upper Cretaceous-Paleocene igneous rocks dredged from the Aves Ridge, Upper Jurassic and lower Early Cretaceous rocks from Desirade Island, as well as kinematic constraints suggest some Mesozoic subduction along the eastern Caribbean plate boundary (Bouysse, 1984).

The forearc of the Lesser Antilles consists of the Barbados Ridge (Fig. 2) flanked to the west by forearc basins, the most prominent of which is the Tobago Trough. This forearc narrows in width from 450 km in the south to less than 50 km in the north; the width at the latitude of ODP Leg 110 coring is about 260 km. The Tobago basin is restricted to the southern half of the arc. To the west, its sedimentary fill thins through progressive on-lap over the eastward dipping island arc basement. To the east, where the thickest sediments occur (Valery et al., 1985), substantial folding and thrusting (?) in pre-Pliocene sediments and moderate folding in the Pliocene to Quaternary sediments reflect the accretion of some forearc basin deposits onto the back of the accretionary prism. Similar back-thrusting and folding also occur at the latitude of the Leg 110 transect (Speed, Westbrook et al., 1984; Ladd et al., 1986). Back-thrusting suggests that compressional deformation is occurring across the whole accretionary prism; numerical modeling supports this observation (Ngokwey, 1984).

The accretionary complex is bounded to the east by the deformation front which is defined as the first occurrence of major megascopically visible tectonic features, such as folds and thrusts. The style of initial accretion varies from south to north according to the sediment thickness on the incoming oceanic crust (Mascle et al., 1986). To the south the incoming sedimentary sequence is several kilometers thick and is deformed into broad eastward verging folds with westward dipping reverse faults or thrusts. To the north, in the Leg 110 area, where the Atlantic sedimentary cover is less than 1000 m thick, the tectonic style is more difficult to resolve seismically owing to the small size of the structures (Fig. 3). The results from Leg 78A (Biju-Duval, Moore et al., 1984) and carefully reprocessed seismic sections suggest that the initial accretion occurs along eastward verging low-angle thrusts that bound moderately deformed and westward-dipping sedimentary packets. Everywhere along the Barbados Ridge the most striking feature is the presence of a décollement separating the accretionary prism from the underlying underthrust sediments. Eighty km north of the Leg 110 area the décollement has been traced at least 70 km west of the deformation front (Westbrook et al., 1982).

The Atlantic abyssal plain just east of the deformation front shallows from more than 6000 m deep in the north to less than 3000 m deep to the south. This bathymetric gradient reflects the

copious sedimentary influx from South America, most of which was deposited during the late Miocene to Holocene, mainly through the Orinoco and Amazon drainage systems (Damuth et al., 1970; Embley et al., 1977). As a result, sediment thickness on the Atlantic Ocean floor decreases from over 7 km south of 11°N to less than 1 km at the latitude of ODP Leg 110 drilling. The basement located 6 km east of the deformation front at 15°N is of Senonian age or younger. South of 12°N the basement is presumably of Late Jurassic-Early Cretaceous age (Westbrook et al., 1984). The Senonian and younger oceanic crust shows WNW–ESE trending fracture zones which are probably remnant transform faults. These faults, which clearly offset magnetic anomalies, appear on the seafloor as troughs and flanking asymmetrical ridges (Peter and Westbrook, 1976). A prominent example of one of these highs is the Tiburon Ridge at about 15°N, on which Site 672 is located.

SEISMIC UNITS, LITHOLOGY, AND BIOSTRATIGRAPHY

The characteristics of the oceanic sedimentary sequences at Site 672 provide a basis for understanding the structural development and hydrogeologic behavior of the accreted complex. The seismic profile CRV-128 (Fig. 4) shows five alternatively transparent and reflective seismic units. The four uppermost units and the top of the fifth were cored at Site 672. The lowermost seismic unit lies on a rough oceanic basement considered to be Senonian age (Late Cretaceous) based on magnetic anomalies (Westbrook et al., 1984). The oldest sediment over the basement is Campanian at Site 543 (Bergen, 1984).

The lower Pleistocene to Pliocene section forms the upper transparent seismic unit, consisting of calcareous clay and mud, marl, and frequent ash layers. Excellent stratigraphic control is provided by rich and well-preserved assemblages of calcareous nannofossils and foraminifers.

The second seismic unit consists of discontinuous, parallel, weak-to-strong reflectors that are generated by significant changes in both lithology and physical properties with respect to the overlying Pliocene unit. The dominant lithology is Miocene mudstone with local ash layers. The disappearance of nannofossils and foraminifers within the Miocene sediments is reflected by a decreased carbonate content relative to the Pliocene sequence. Accordingly, the detailed stratigraphy is poorly constrained except in the lower Miocene section where a well-preserved radiolarian assemblage occurs. This lower Miocene section also records higher bulk porosity relative to the surrounding sediment (Fig. 4), presumably related to its high radiolarian content. This interval also includes en-echelon dilatant veins and related subhorizontal shear zones; the remaining cores of the entire hole show high-angle normal faults only.

The Neogene section at Site 672 is very similar in facies and thickness to that at Site 543, 20 km to the north. Both sections represent slow hemipelagic accumulation in an open oceanic environment below and above the CCD. Occasionally episodic influxes of volcanic ash from the Lesser Antilles volcanic arc are also recorded in the sediments. Most of this Neogene section is accreted at the deformation front as the décollement zone develops in the anomalously porous lower Miocene sequence. The Neogene sediments from the accretionary complex show facies similar to the one cored at Site 672. Slight differences in thickness (Fig. 5) may result either from local variation in initial sedimentation rates, or from small unrecognized structural duplications.

The third, acoustically transparent seismic unit consists principally of Oligocene interbedded claystone, calcareous claystone and mudstone, marl, and thin silt layers. Ash layers are absent. Moderate-to-good preservation of nannofossils and foraminifers provides good stratigraphic control; radiolarians are scarce and poorly preserved.

The upper and middle Eocene section is formed of distinctive cyclic alterations of claystone, laminated calcareous mudstone and marl, micritic limestone and calcarenite, and glauconitic sand. This fourth seismic unit comprises prominent, moderately strong and continuous reflectors. Calcareous fossils are

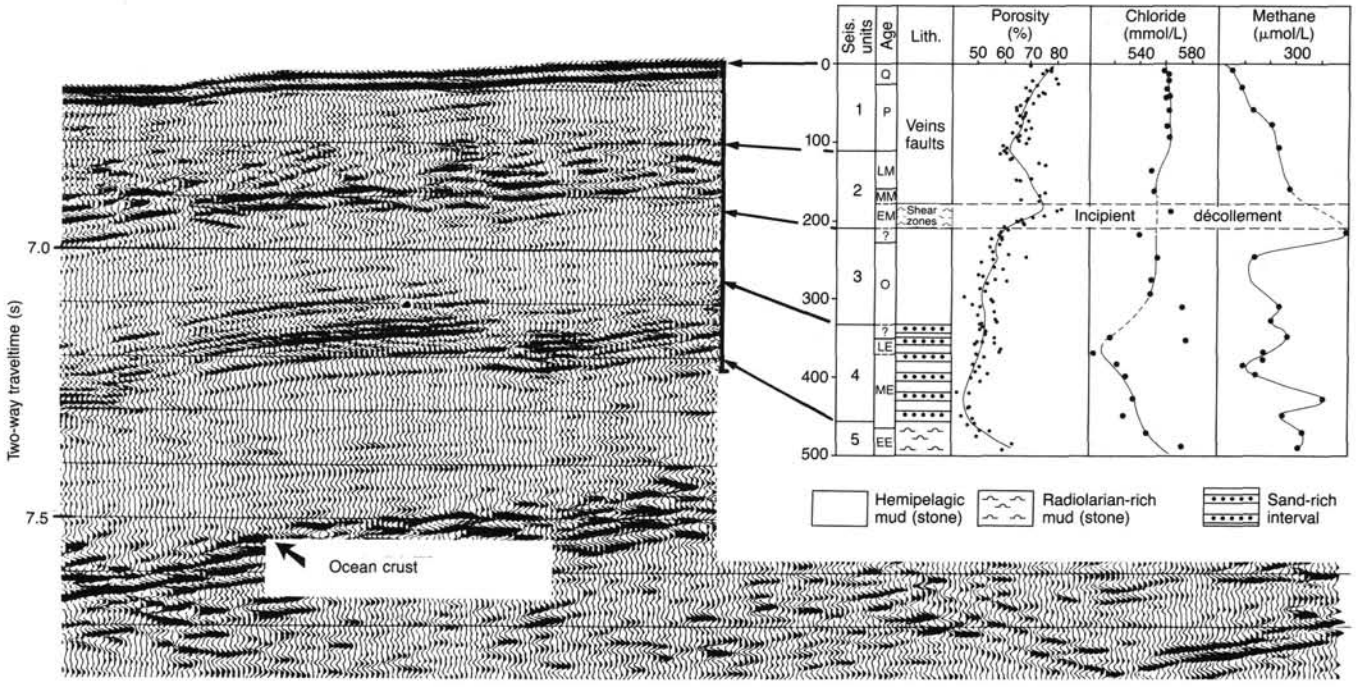

Figure 4. Detail of seismic line CRV 128 in vicinity of Site 672 showing the correlative lithology, physical properties, and pore-water compositions of the five seismic units penetrated at this site.

moderately well preserved through the base of the middle Eocene.

The lowermost middle Eocene and lower Eocene show a sharp increase in porosity and water content which is correlative, as for the lower Miocene interval, with an increase in radiolarian content. Radiolarians provide good stratigraphic control in spite of their poor state of preservation. Calcareous fossils are absent. This section is correlated with the top of the lower transparent seismic unit. A Campanian age is inferred for the basal part of this unit, based on the results from DSDP Site 543.

The middle Eocene to upper Oligocene section cored at Site 672 is 3.5 times thicker than the one drilled at Site 543, where only clays and radiolarian clays were recovered. The relatively high sedimentation rate at Site 672, as well as the diversified lithologies encountered, are probably a result of terrigenous and biogenic influxes from the South American continent and from the upper portion of the Tiburon Rise. Although most of the Site 672 section is fine-grained and of low permeability, the sand layers of the middle Eocene to lower Oligocene interval have high primary porosities and permeabilities which may have facilitated fluid flow up-dip from beneath the accretionary prism (see discussion below).

STRUCTURAL FEATURES

General Framework

Structural features at the toe of the accretionary complex are well expressed on the Seabeam map and on the seismic profile (Fig. 3, see backpocket figures). A narrow linear trough deepening slightly to the north marks the deformation front that separates the accretionary prism from the Tiburon Rise of the Atlantic abyssal plain (Fig. 1). The seafloor morphology is generally smooth to the east. The bathymetric changes along the deformation front and the few northwest to southeast-oriented highs directly reflect the northwest deepening and normal faulting of the incoming oceanic crust. The rough morphology to the west is suggestive of active seafloor deformation. The general forearc slope is to the northeast, but small-scale north–south features, such as ridges or slight increase in the slope gradient, occur. Similar to the larger scale features of the southern Barbados Ridge (Biju-Duval et al., 1982), the north–south ridges can be correlated with active thrusts.

West of the deformation front three acoustic units are apparent on the seismic profile (Fig. 3; backpocket Figure 5, this volume). The upper unit shows a few westward-dipping reflectors which are locally difficult to differentiate from diffraction hyperbola remaining after migration. Some of these reflectors correlate with thrust faults dipping moderately to the west. This upper seismic unit encompasses the accretionary complex and is bounded at the base by a major reflector representing the top of the décollement zone. This décollement is nearly parallel to the bedding in the subjacent underthrust sequence. The décollement zone was sampled at Sites 671, 541, 675, and 676 where it consistently occurs in lower Miocene sediments. The shear zones in stratigraphically correlative sediments at Site 672 suggest oceanward propagation of the décollement zone.

Below the accretionary complex, seismic units three, four, and five comprise underthrust sediments. Although the uppermost unit below the décollement zone shows minor truncations from shotpoint 600 to 800, no down-stepping of the décollement zone is apparent on seismic line CRV 128. Normal faults trending northwest–southeast and northeast–southwest offset the top of the oceanic crust. As displacements diminish in the middle to upper Eocene deposits, fault activity is probably related to the early history of the oceanic basin.

Initial Accretion: Imbricate Thrusting at Sites 671, 675, 676, 541, and 542

Correlations of the repeated stratigraphy of Sites 671 and 676 (ODP Leg 110) and Sites 541 and 542 (DSDP Leg 78A) with seismic line CRV 128 clearly indicate that initial offscraping occurs in the style of imbricate thrusting (Figs. 3, 5, 6). The structural features of the cores, however, reflect small-scale complications.

Drilling at Site 671 recovered 500 m of Pleistocene-to-lower Miocene imbricately thrusted calcareous mud and mudstone (Figs. 5 and 6). At 128 mbsf a biostratigraphic inversion of upper Miocene over lower Pleistocene sediments defines a low-angle reverse fault with a throw of 160 m. The fault is only a 5-mm-wide shear zone of brown mud. The Pliocene section above the thrust has suffered gentle folding as indicated by bedding dips up to 40°, but the upper Miocene beds immediately above the fault are flat-lying. Lower Pleistocene sediment in the core below the fault shows at least one vertical bedding dip, whereas the next cores below exhibit horizontal bedding dips. This thrust fault can be correlated with a weakly-defined, short reflector dipping about 15° to the west, which is shallower than the dip of approximately 50° observed in the core. At greater depth, an unusually thick nannofossil zone and an interval of pervasive scaly fabric development and intense brittle faulting at 375 mbsf suggest reverse faulting. A possible biostratigraphic inversion occurs over an interval from 435 to 482 mbsf and may be related to a scaly zone at 447 mbsf. This possible fault is correlated with a weak reflector that may be traced to a biostratigraphically defined fault at Site 541 (upper Miocene over Pliocene). In the imbricately thrusted section (0 to 500 mbsf), bedding dips show a random distribution between 0 and 90° with an average value of about 20°. However, from 128 to 500 mbsf, i.e., below the first major thrust fault, this average value rises to about 30° with a cluster of higher values (60°) between 300 and 425 mbsf. In this imbricately thrusted section (0 to 500 mbsf) numerous reverse and normal faults, and six distinct zones of scaly cleavage are visually apparent.

Features similar to those documented at Site 671 were previously encountered at Sites 541 and 542 of DSDP Leg 78A (Fig. 5). At Site 541, a major thrust at 276 mbsf emplaces upper Miocene over middle Pliocene sediment; two smaller faults at 172 and 263 mbsf repeat lower Pliocene and upper Miocene intervals, respectively. At Site 542, stratal disruption, slickensides, and an anomalously thick single nannofossil zone at 250 to 325 mbsf argue for thrusting and a total stratigraphic repetition of about 70 m. At both sites the average bedding dip is 13° with maximum values of 30°, i.e., slightly less than at Site 671, which is located less than 1 km upslope.

Site 676, located 250 m arcward from the deformation front, records some of the earliest effects of offscraping (Figs. 5, 6). Three zones of active deformation occur in this single vertical section. Tight folding of Pleistocene sediments (with bedding dips up to 75°) and a small-scale reverse fault at about 30 mbsf probably represent the shallow expression of the frontal thrust of the accretionary complex. A correlative weak but continuous arcward-dipping seismic reflector emerges at the surface in the exact location of the deformation front. A biostratigraphically defined thrust fault and an associated zone of scaly fabric at 210 mbsf repeats an upper Miocene interval about 30 m thick. A correlative weak seismic reflector at this depth has roots in the décollement. This fault apparently represents a newly propagating frontal thrust, the surface expression of which may be the small bulge on the seafloor about 3 km east of the present formation front. The deepest tectonic features observed at Site 676 are dilatant veining, incipient subhorizontal shearing, and an associated biostratigraphic inversion at 271 to 305 mbsf. These

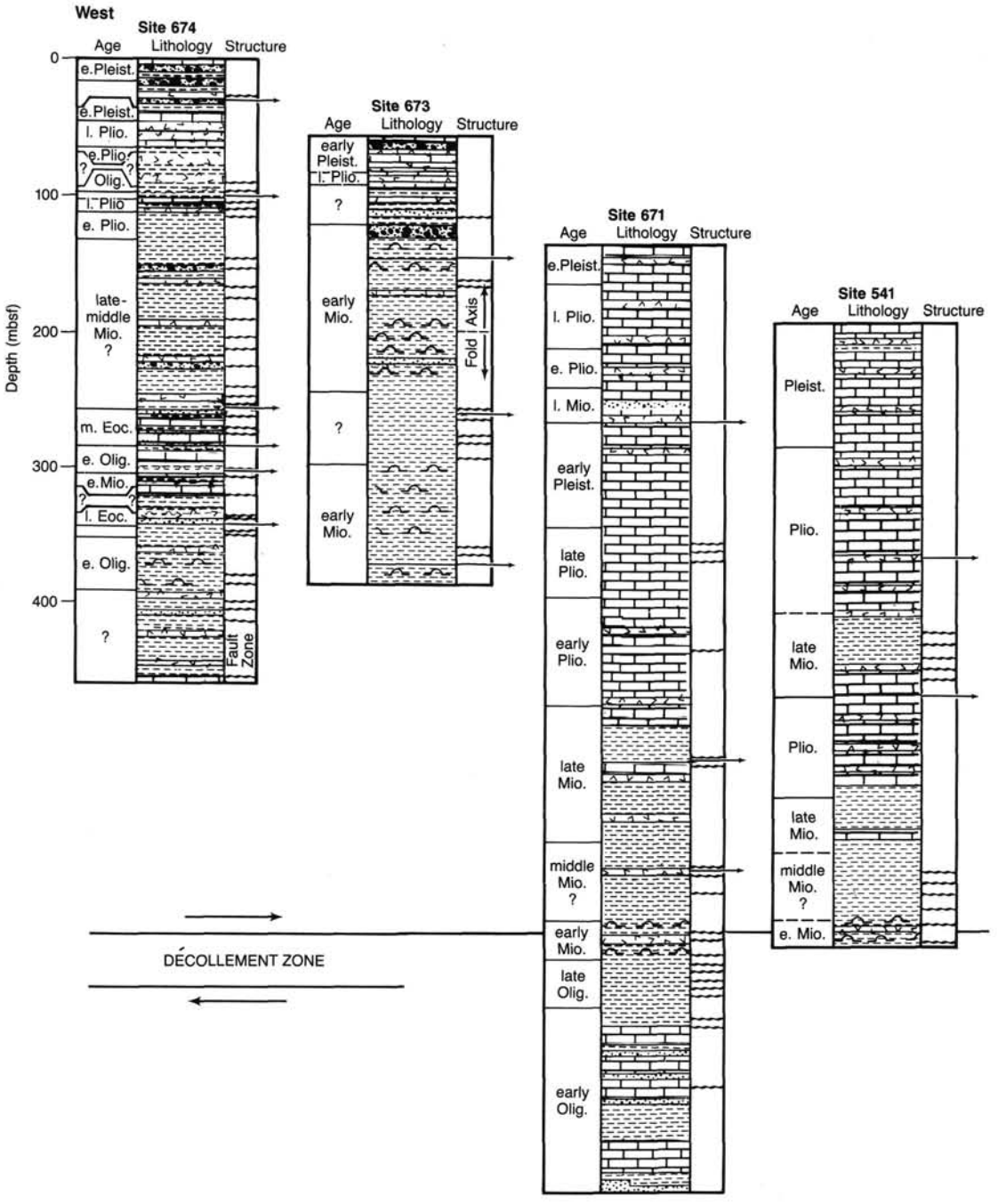

Figure 5. Stratigraphic summary of Leg 110 and Leg 78A holes along seismic line CRV 128.

features occur in the lower Miocene interval and are interpreted as the oceanward propagating basal décollement, in good agreement with the seismic correlation from Site 672 to Site 671. The average bedding dip value in the Pliocene and Miocene section above the décollement is about 8°.

A cross-section, based on the combined interpretation of the seismic and drilling data from Site 671 through 676, suggests a series of shallowly westward-dipping thrust faults, bounding little- to moderately-deformed sedimentary packages (Fig. 6). Four major thrust faults are recognized westward from the deformation front through Site 671, each having a surface expression on the seafloor. A thrust is probably propagating from the décollement seaward below the present frontal thrust.

Décollement

The décollement zone is seismically defined near the deformation front where the sediment on the incoming oceanic plate is bifurcated into offscraped and underthrust portions (Fig. 3). In a sense, the décollement zone marks the plate boundary between the underthrusting Atlantic Ocean crust and the overlying Caribbean Plate. The décollement zone begins at a depth of about 200 mbsf but progressively deepens to the west, reaching about 1350 mbsf beneath Site 674 (assuming an interval velocity of 1800 m/s for the overlying accretionary prism). The décollement is a zone of deformation at Sites 671, 675, 676, and 541, not a discrete surface.

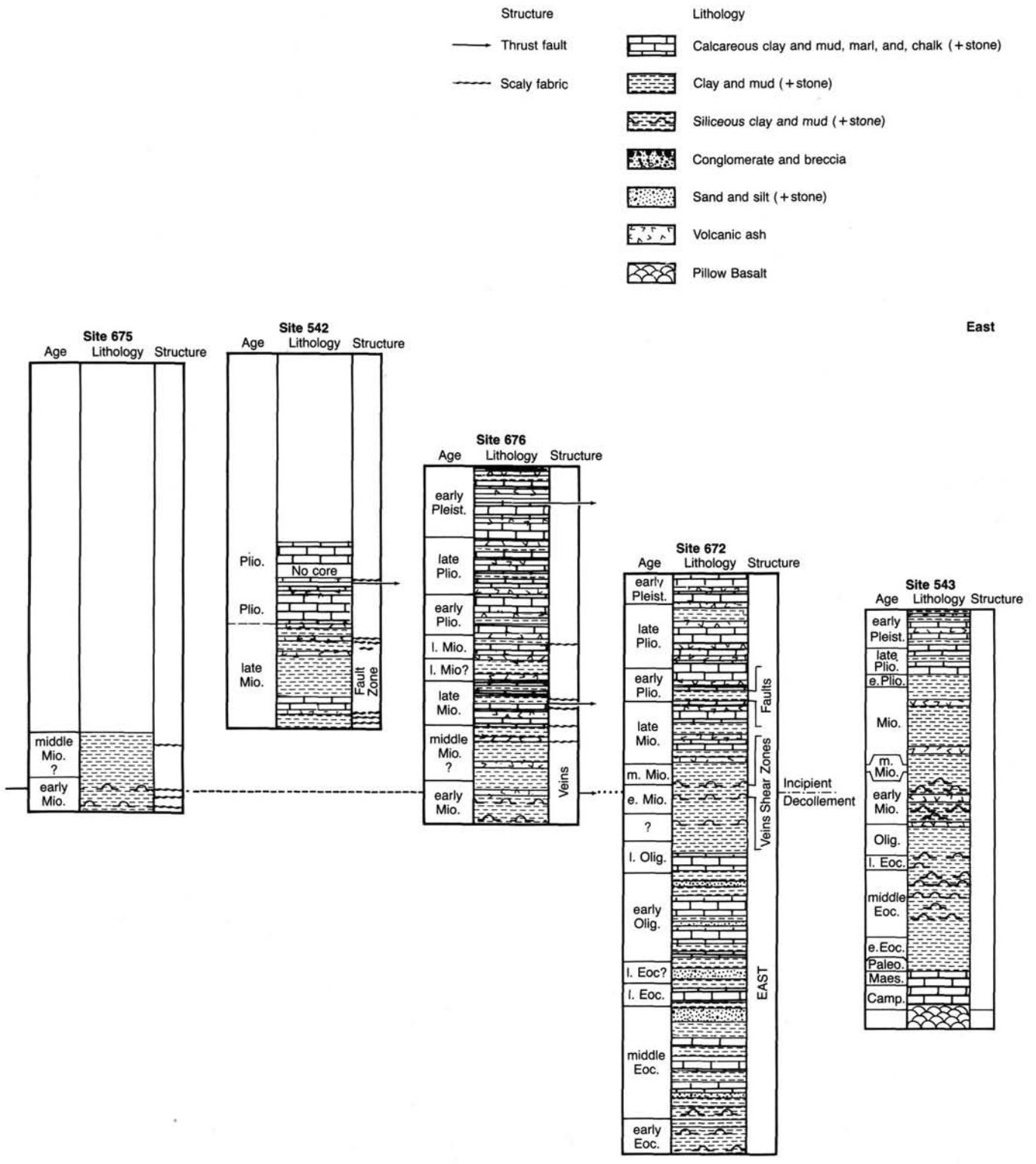

Figure 5 (continued).

The décollement zone at Site 671 is not defined by a biostratigraphic inversion but by a strongly developed zone of scaly fabric extending from 500 to 540 mbsf (Fig. 5). The dominant attitude of the scaly foliation is at moderate angles to the core axis. The intensity of the scaly fabric decreases with depth. The host beds of the décollement zone are of early Miocene to late Oligocene age. Radiolarian-bearing brown to olive gray claystones characterize the lithology of the décollement zone. At Site 671, scattered pale gray 1 to 2-mm spherules of clinoptilolite occur in the décollement zone along with a single 1-mm-thick shear vein of "zeolite."

The décollement zone was also successfully cored at Site 675 in an interval of interlayered orange brown siliceous mudstone and olive-to-olive brown, nonsiliceous to siliceous mudstones of early Miocene age. The orange brown portions contain common black manganese concentrations and small (1 mm diame-

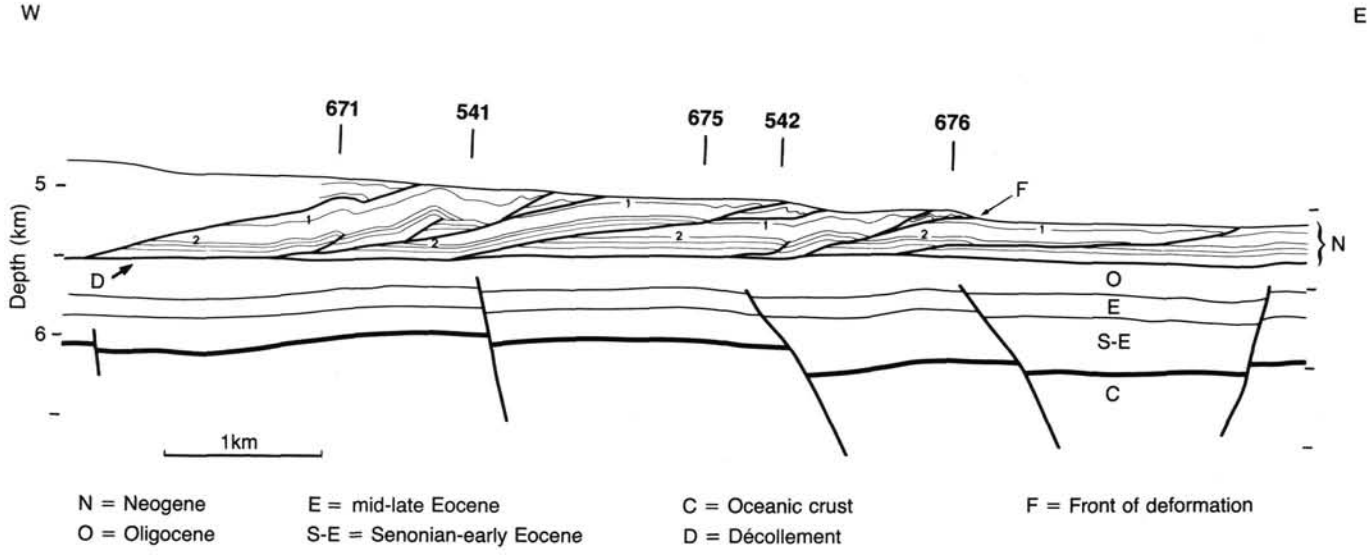

Figure 6. Cross-section through the zone of initial accretion. Section is based on all available drilling and seismic data. Numbers on section (1 and 2) correspond to the lower boundaries of seismic Units 1 and 2, respectively.

ter) white spherules of clinoptilolite. Scaly fabric occurs throughout the upper section of the décollement zone. Centimeter-length rhodochrosite-filled veinlets overprint the scaly fabric. One of the veins is cut off by a low-angle fault and another one was found to have a surface with dip-slip slickensides. Apparently deformation mechanisms may locally evolve from scaly fabric development to dilatant veining with accompanying and subsequent brittle shearing. The veining also suggests that the décollement hosted nearly lithostatic fluid pressures to allow dilatant failure and crack-sealing in the scaly claystones.

The top of the décollement at Sites 671 and 675 correlates with the same strong but discontinuous reflector seen on line CRV 128. This reflector also corresponds to the décollement reached at the bottom of Site 541. In these three cases, the top of the décollement occurs in lower Miocene brown radiolarian mudstone or claystone. When followed to the east, this reflector perfectly corresponds to the lower Miocene interval cored at Sites 676 and 672. In both cases, this interval is characterized by mud-filled veins and low-angle reverse faults which indicate an incipient subhorizontal shearing in a regime of high fluid pressure. We believe these structures indicate a seaward propagation of the décollement zone from the base of the accretionary complex. Moreover, the compressive stress regime of the encroaching accretionary complex apparently propagates at least 6 km seaward of the deformation front to Site 672.

Underthrust Sequence

About 150 m of the underthrust sequence was cored below the décollement zone at Site 671. These sediments consist of cyclic alternations of calcareous and noncalcareous mudstones or claystones, marlstones and silty intervals (Fig. 5). The hole bottomed in unconsolidated, fine- to medium-grained glauconitic quartz sand. The entire cored section is of Oligocene age and lithologically similar to the Oligocene interval recovered at Site 672. The underthrust sequence below the décollement zone shows a gradual downward decrease in the frequency of scaly fabric. Horizontally to shallowly dipping faults of unknown displacement occur at two levels. Average bedding dip is about 5°, in good agreement with the seismic data that show shallowly dipping reflectors. At Site 671 the underthrust sequence is located 4 km arcward of the deformation front, but it appears to have suffered only minor deformation, most of the displacement being accommodated along the 40-m-thick décollement zone.

Upslope Consolidation

In addition to penetrations near the deformation front, we drilled two sites, 12 and 17 km upslope and west of the deformation front, to measure the continuing evolution of the offscraped sediments (Fig. 5). A moderate slope cover here suggests subjacent sediments were accreted in the Pliocene. At Sites 673 and 674, sediments are far more deformed than near the deformation front, and include structural features similar to those occurring in subaerially exposed accretionary complexes such as Barbados Island (Speed, 1983; Torrini et al., 1985). This intensity of deformation was achieved with only modest dewatering, in sedimentary deposits with about 50% porosity.

At Site 673 we penetrated a total of 330 mbsf, including a slope cover about 75 m thick with debris flow and slump deposits (Figs. 5, 7). Below the slope cover we sampled four internally deformed packets of Miocene sediment separated by three biostratigraphically defined thrust faults. These faults have tentatively been correlated to discontinuous arcward-dipping reflectors (on lines CRV 128 and A3) which appear to be related to slight changes in P-wave velocity and bulk density (Fig. 8). The second packet shows a conspicuous large anticlinal fold with an overturned lower limb where bedding dips are in excess of 40°. This fold is bounded along its base by a scaly zone about 20 m thick that probably corresponds to a major thrust. Additionally, the base of this fold is characterized by calcite veins, which suggest that this zone of carbonate-free claystones experienced high fluid pressure. The calcite veins locally occur along the scaly fabric, indicating that the latter may function as a fracture permeability. Veins also cross-cut the scaly fabric. Between faults, calcite and mud-filled veins occur in a variety of orientations, locally forming a network or anastomosing pattern. The absence of major faulting in brown claystones of early Miocene age cored at 260 mbsf suggests that the décollement surface was positioned at a deeper stratigraphic interval during offscraping at Site 673.

Definitive evidence of a stratigraphically lower décollement zone was obtained upslope at Site 674 where two of the three thrust-bounded tectonic units drilled yielded rocks of Paleogene age (Fig. 5). The upper, about 100 m thick, tectonic unit consists of a 10-m-thick, sheared, lower Oligocene to lower Miocene, overturned section. This is overlain by 90 m of slope deposits, including debris flow and slump material from upslope. Reverse faulting and dilatant veining are obvious in this slope

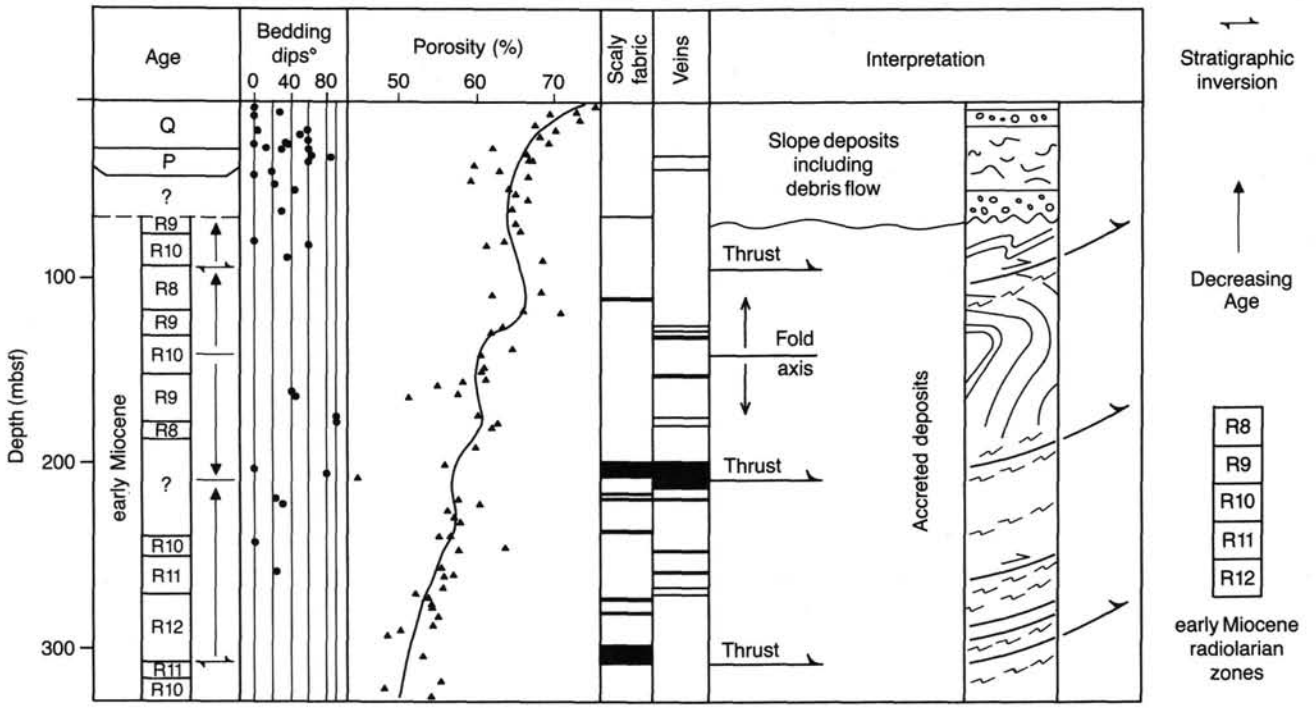

Figure 7. Structural features and porosity data from Site 673. Decreasing age directions and biostratigraphic inversions are in each case determined from radiolarian zonations in lower Miocene sediments.

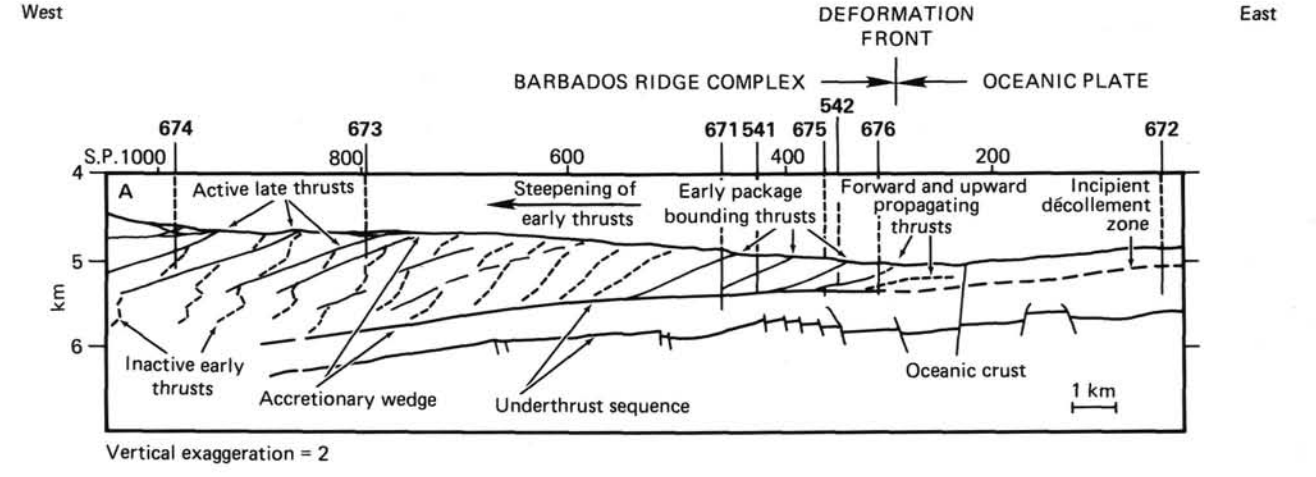

Figure 8. Schematic cross-section along seismic line CRV 128 showing zone of initial accretion at deformation front with continuing deformation and late (out-of-sequence) thrusting upslope near Sites 673 and 674.

cover, indicating that it is in the process of being tectonically incorporated into the accretionary complex. The second tectonic unit is formed of generally steeply dipping (60° and more) upright, lower Miocene to upper Miocene strata. Well-developed scaly fabric in this unit generally dips at angles similar to the bedding, and may represent bedding-parallel thrusts. The proportion of the cores composed of scaly fabric increases downhole until it is well above 50%. Calcite veining is also increasingly abundant in the deeper zones of scaly fabrics. The third and deeper tectonic unit is made of at least five packets of rocks yielding ages from middle Eocene to early Miocene. Bedding dips are variable in these units but are predominantly below 50°. Tight folding is obvious in the upper middle Eocene sand-bearing sequence. This third tectonic unit probably encompasses a complexly faulted and partially overturned limb of a large recumbent fold. Alternatively, it could also be interpreted as an aggregation of upright packets bounded by originally low-angle flat and ramp structures that have been rotated to steep orientation during imbrication or folding.

The low-angle faults forming the boundaries to tectonic units show well-developed scaly fabric but little veining. They mark significant changes in acoustic impedance and can tentatively be correlated to arcward-dipping, discontinuous, weak reflectors. The upper fault at Site 674 emplaces lower Oligocene to lower Miocene sediments over upper Pliocene strata, resulting in the largest stratigraphic inversion known from ODP-DSDP drilling. The lower fault emplaces lower Miocene strata over lightly folded middle Eocene strata. This fault could be interpreted as having

a normal displacement across it on purely stratigraphic grounds. However, no normal offsets were seen in any part of the section at Site 674. Furthermore, the intensity and form of the fabric in the fault zone were similar to those associated with thrust faults. The thrust fault interpretation requires the fault to have cut through an already structurally complex sequence. This shallowly dipping fault, as well as the overlying fault, are thus interpreted as late (or out-of-sequence), second-generation structures that deformed sediments that were already imbricated.

Sediments cored at Sites 673 and 674 record a history of continuing deformation in the accreted sediments during their progressive uplift. The sites show a significant slope apron that includes resedimented material derived from upslope. Late or out-of-sequence thrust faults appear to correlate with the landward-dipping reflectors (Fig. 8). The substantial deformation documented at Sites 673 and 674 is achieved with only modest dewatering.

PHYSICAL PROPERTIES

Physical properties measurements conducted on the Leg 110 cores include water content, bulk density, grain density, porosity, sonic velocity, shear strength, thermal conductivity, and formation factor. Here we emphasize the porosity data as it provides a direct indicator of the magnitude of dewatering and consequently is relevant to the hydrogeology.

A composite depth-porosity plot of data from all Leg 110 and Leg 78A sites reveals little apparent variation between the oceanic reference sites (Sites 543 and 672) and those located on the accretionary prism (Fig. 9). All sites show a general decrease in porosity with respect to depth. Local variations in the porosity curves are principally related to lithology.

Combination depth-porosity plots of specific age intervals for a number of sites (Fig. 10) resolve volume changes owing to vertical and lateral loading. A plot of data from Pliocene sediments from all sites shows a decrease in porosity with depth similar to that apparent in Figure 9. Pliocene sediments at Site 671 have been repeated by thrusting with one package remaining near its original depositional depth and another being buried an additional 200 m owing to thrust imbrication. In comparison to Site 672 on the oceanic plate, the Pliocene package that experienced no change in burial has decreased its porosity about 3.4% with an accompanying decrease in volume of 9% (since porosity equals volume of voids over volume of voids plus solids, a change in porosity is not equal to the change in total volume of the sediment). This volumetric decrease reflects tectonic dewatering owing to lateral stresses. Conversely, the Pliocene section with the additional 200-m burial decreased in porosity 13.8% and volume 29% owing to both the effects of lateral stresses and the loading due to burial. The total volume reduction of the accreted sediments measures the volume of fluid generated during the deformational process. For example, the sediments of the accretionary prism and décollement zone (Quaternary through lower Miocene) at Site 671 have undergone a respective porosity and volume decrease of 9.1% and 22% relative to sediments of the same age at Site 672.

A porosity-depth plot for lower Miocene sediments shows a porosity decrease of 10.7% from Site 672 to Site 671 with an associated volume reduction of 26% as these materials are underthrust in the décollement zone (Fig. 10). Conversely, Oligocene sediments lying below the décollement showed only a 2.7% change in porosity from Site 672 to 671 with a volume decrease of 6%. Both sequences have been subjected to equivalent change in burial depth owing to loading by the accretionary prism. The enhanced dewatering of the lower Miocene sediments probably results from their less advanced initial consolidation state, their position directly in a dewatering conduit (short drainage path), and their considerable deformation, perhaps leading to "shear dewatering" (Karig, 1986).

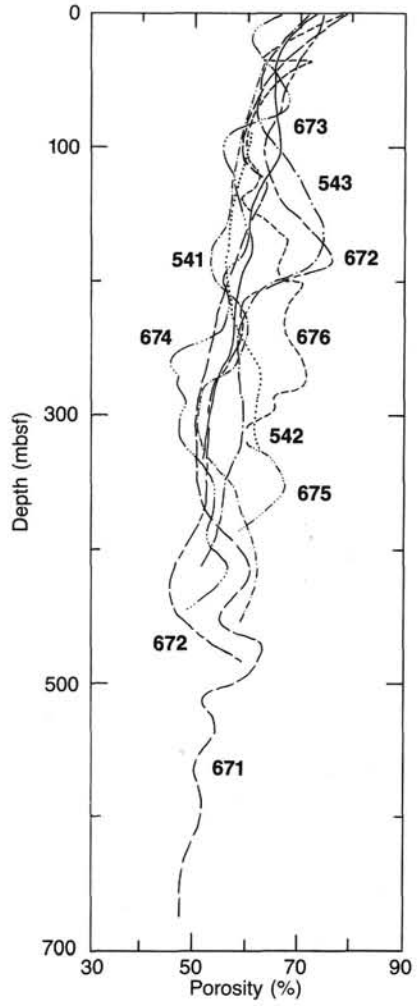

Figure 9. Summary of porosity data for all sites from Legs 78A and 110. Note small difference in porosity values between sites with essentially undeformed sedimentary sequences on the oceanic crust (Sites 543 and 672) and those penetrating the accretionary prism and underthrust sequence.

Overall, the magnitude of dewatering associated with accretion and underthrusting is only moderate, even in sediments as far arcward as those at Site 674. The fine grain size and consequent low permeability have apparently limited fluid expulsion, suggesting low effective stresses and high pore pressures. Even though the sediments at Site 674 are considerably deformed, their remaining high porosity indicates the potential for significant additional collapse of the sediment framework, with consequent fluid expulsion during continued structural evolution.

GEOCHEMISTRY

During Leg 110 major efforts were focused on the chemistry of the pore waters with related analysis of organic geochemistry and mineralogy of the sediments. Key questions include the degree of sediment-water interactions and whether the fluids were exotic or of local origin. Shipboard pore waters were analyzed for chloride, calcium, magnesium, ammonia, silica, sulfate, and methane. Additionally, organic and inorganic carbon contents and bulk mineralogy were determined. Here we focus on the measurements of methane and chloride, which provide essential insights into the relationship of fluid flow and the major structural features.

Plots of methane concentrations in pore-water samples define methane-bearing and methane-free fluid realms (Fig. 11).

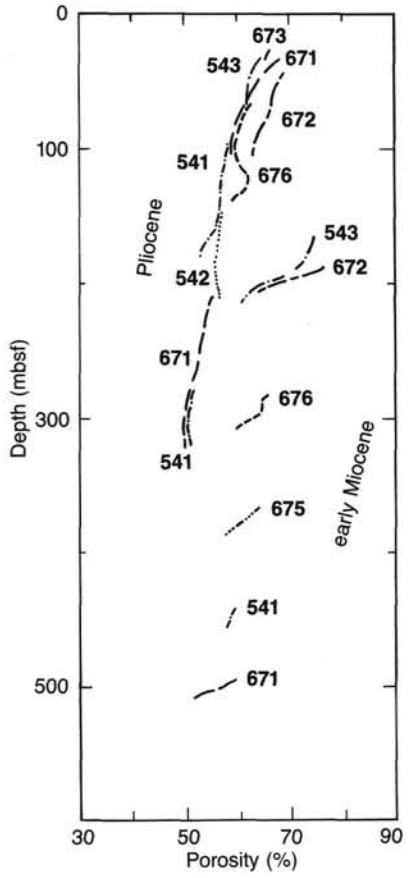

Figure 10. Porosity values from all Pliocene and early Miocene age sections to illustrate trends of dewatering in accretionary prism and along décollement zone, respectively.

The methane-free region occurs in the accretionary prism above the décollement zone, whereas methane-bearing fluids are restricted to the décollement zone and the subjacent underthrust sediments. Fluid compositions show smaller-scale variations related to specific structural and stratigraphic features. For example, the methane content of the pore fluids is negligible throughout the accretionary prism at Site 671 until the décollement zone is approached; there the methane concentrations reach a local maximum (Fig. 11). The methane content decreases below the décollement zone but rises again with approach to a permeable sand layer at the base of the hole. Similar methane anomalies are observed at Site 676 around faults that splay up from the décollement zone, at Site 672 along the stratigraphic projection of the décollement zone, and to a lesser degree within the sandy interval below (Fig. 11).

Profiles of chloride content tend to show negative anomalies associated with faults and the permeable sand layer of the underthrust sequence (Figs. 11, 12). For example, a chloride minimum occurs in the décollement zone at Site 671 and a series of low values are found as one approaches the permeable sand layers below. At Site 674, negative chloride anomalies are associated with three of five faults (Fig. 11), suggesting that along some but not all faults fluid migration is sufficient to produce geochemical signatures. Negative chloride anomalies at Site 674 not associated with faults may reflect undocumented shear surfaces.

Overall, pore-water chloride concentrations decrease with measured sub-bottom depth and upslope across the accretionary prism (Fig. 12). This relative freshening of the pore fluids may reflect the effect of long-term flow of low-salinity fluids through the many faults cutting the accretionary prism, with consequent diffusion of more saline pore fluids to unfaulted areas.

The negative chloride anomalies may be generated by an ultrafiltration process in which the clays act as semipermeable membranes, selectively passing water but restricting the motion of some ionic components (Hanshaw and Coplen, 1973). The generally smectitic nature of the Leg 110 sediments, their high clay content, and appropriate (moderate to low) water content maximize the opportunity for ultrafiltration (Kharaka and Berry, 1973). Chloride is very sensitive to ultrafiltration and therefore a good marker of this process. Dehydration of smectites at depth may also explain the low-chloride waters associated with the deeper fault zones and the middle Eocene and lower Oligocene permeable sand layers. The chloride anomalies might have been produced by the melting of gas hydrate, a process documented in studies of the slope sediments of the Middle America Trench (Gieskes et al., 1984). However, the extremely low concentrations of methane and the lack of bottom-simulating reflectors suggest that the presence of hydrate is unlikely.

Notable negative anomalies in chloride are associated with the décollement and zone and basal permeable sand layer cored at Site 671. The magnitudes of the chloride anomalies at the same structural and/or stratigraphic levels at Sites 676 and 672 are much less pronounced, although methane concentrations are everywhere similar. Apparently generation of a chloride anomaly requires significant dilution of the large existing reservoir of chloride normally present in seawater. Conversely, detection of a methane anomaly requires measurement of only a small amount of this dissolved constituent against a background in which it is absent. Therefore, methane, where present, is a much more sensitive indicator of fluid flow. Peter Vrolijk's preliminary carbon isotope data (pers. comm.) indicate that the methane detected in Leg 110 samples is of thermogenic origin. Conditions appropriate to thermogenic methane formation were not found in the drilled holes; they probably exist deeper within the accreted prism. The distinct localized concentration gradients in pore water samples define a methane-bearing and methane-free fluid realms (Fig. 11). The methane-free region occurs in the accretionary prism above the décollement zone, whereas methane-bearing fluids are restricted to the décollement zone and the subjacent underthrust sediments.

HEAT FLOW

Temperature measurements were made at most holes during coring to relatively shallow depths with the hydraulic-piston core tool. Temperature measurements were continued to substantial depths at Sites 674 and 676 using the WSTP tool. Thermal conductivity was routinely collected on all cores.

Overall, the observed conductive heat flow values exceed those expected due to conductive heat transfer from oceanic crust formed 90 Ma (Fig. 13; Anderson and Skilbeck, 1982). Conductive heat flow calculated for each hole in some cases shows two values where the temperature gradient changed downhole. Changes in downhole temperature gradients at Sites 674 and 676 are associated with faults, suggesting that the gradients are caused by flow of warm fluid along the faults (Fig. 11). Warm fluids could act as a heat source, raising the temperature of the adjacent sediment, and explaining the nonlinear thermal gradients. Heat flow calculations indicate that nonlinear thermal gradients observed at Sites 674 and 676 would decay in hundreds to a few thousand years without resupply of warm fluid along the faults.

The heat flow data in Figure 13 represent the amount of heat being transferred conductively. The warm deeply derived fluid found anomalously close to the cold sediment/water interface produces the enhanced conductive heat flow, but only represents

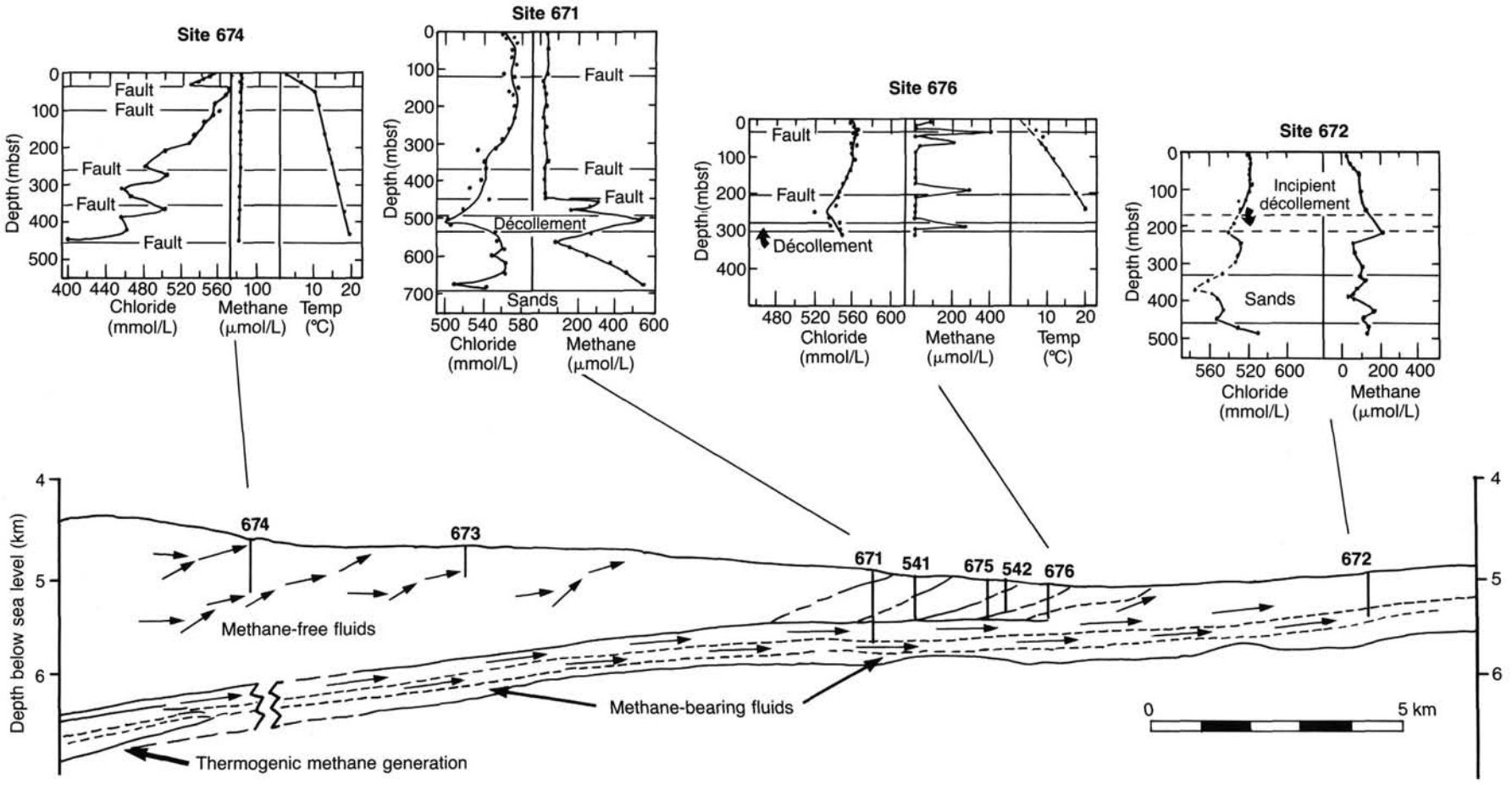

Figure 11. Plots of methane and chloride concentrations in pore waters, and temperature gradients from selected sites. Note that methane anomalies are restricted to intervals below the décollement zone, defining a methane-bearing fluid realm. The virtual absence of methane in the accretionary prism defines the methane-free fluid realm.

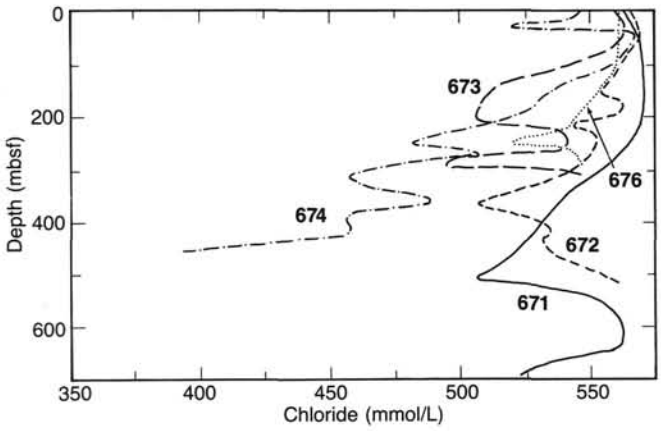

Figure 12. Composite plot of chloride vs. depth for all Leg 110 sites.

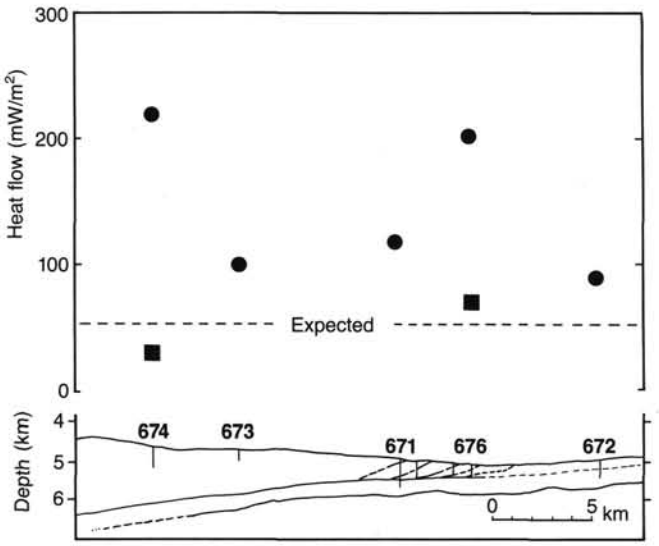

Figure 13. Heat flow measurements from Leg 110 sites. Circles represent single measurements whereas squares represent a second downhole determination of heat flow encountered after crossing a fault (see Fig. 11). The expected heat flow value is that derived from conductive heat transfer from oceanic crust 90 Ma (Anderson and Skilbeck, 1982).

a portion of the total heat transfer. The convective heat flow, actually due to the moving water, can only be established if flow velocities are known.

HYDROGEOLOGY

Elucidation of the hydrogeology of the northern Barbados Ridge was one of the principal goals of Leg 110. Although failure to obtain packer and logging data limited the scope of our investigations, integration of seismic reflection, geochemical, heat flow, physical property, and structural data has defined the hydrological framework of this accretionary prism.

Changes in porosity provide a measure of the magnitude of dewatering and the amount of locally derived fluids. For example, at the position of Site 671, the accreted sediments and those deforming in the décollement zone have lost an average of 22% of their original volume. Less dewatering has occurred below the décollement, where the underthrust Oligocene section has been reduced in volume by only 6%. Several lines of evidence indicate, however, that not all the fluid is locally derived.

Methane of thermogenic origin indicates a deep source for fluid in the décollement zone and the underlying permeable sand layer. A maturity calculation considering both time and temperature (Waples, 1985) at an average thermal gradient of 30°C/km suggests that the threshold of thermogenic methane generation would not be reached until sediments are underthrust at least 30 km arcward of the deformation front. Long-distance migration and relatively deep sources apparently are required for some of the fluid. The declining chloride values in the more arcward sites of the accretionary prism may reflect continuing intrusion of low-salinity fluid through the accretionary prism during its progressive uplift. Thus both patterns of methane and chloride distribution argue for flow of exotically derived fluid through the drilled sections. The measured decreases in sediment pore volume are minimum volumes of flow.

The association of pore-water and temperature anomalies with faults suggests that these are the principal paths of fluid transport in the accretionary prism and décollement zones. In the underthrust sequence the pore-water anomalies suggest that the permeable sand layer is a major conduit for expulsion of fluids. The low permeability of the fine-grained sediments (Marlow et al., 1984) associated with the décollement and faults in the accretionary prism precludes flow through intergranular pathways. Apparently the scaly fabric of the faults acts as a fracture permeability; veins precipitated in the scaly fabric attest to fluid flow along these surfaces.

The localization of methane-bearing fluids within and below the décollement zone indicates that the accretionary prism is a barrier to vertical flow. Given the probable near-lithostatic fluid pressures along the décollement zone (Moore and Biju-Duval, 1984; Davis 1984), the expected development of steep hydrofractures and large-scale flow along a shortened path directly to the overlying seafloor does not occur. Rather, the fluids flow along a much lower hydraulic gradient out the décollement to the seafloor. Apparently the fracture permeability in the décollement zone provides much less resistance to flow than any pathways through the sediment in the overlying prism. Moreover, the probable shallow dip of the maximum principal stress in the accretionary prism (Davis, 1984) would favor opening of shallowly inclined hydrofractures, more nearly parallel to the décollement, rather than steeply dipping hydrofractures through the accretionary prism.

The overall driving force of fluid expulsion within the accretionary prism results from increased total stresses owing to both the vertical stacking of the thrust sheets and, to a lesser degree, the lateral shortening of the prism. The arcward thickening of the accretionary wedge causes an increase in total stress on sediments below the décollement and probably an increasing hydraulic head, driving the fluid up the subduction zone and seaward to at least Site 672. In both cases the increased total stress is probably initially carried by the fluid, resulting in elevated pore pressures. Slow collapse of the sediment fabric, mediated by the low primary permeability of the sediments, results in a decrease in the pore pressure, a transfer of an increasing portion of the total stress to the sediment fabric, and an increased effective stress.

Fluid flow along faults is apparently episodic. Some but not all faults with geochemical anomalies have thermal anomalies. The presence of the thermal anomalies suggests fluid flow within the last 100- to several 1000-yr range (Carslaw and Jaeger, 1959) whereas the geochemical anomalies indicate fluid flow since 100–200 thousand years ago (Gieskes, 1975). The presence of few thermal anomalies but the common geochemical anomalies suggest a periodicity of fluid flow greater than hundreds to a few thousand years but less than several hundred thousand years.

Inferred fluid flow into the faults indicates that they are regions of lower fluid potential than the adjacent source sedi-

ment, at least during part of their movement history. Yet to function as faults they must be weaker than the surrounding sediment, either owing to their lower coefficient of friction or higher fluid potential. It is arguable whether the deformed sediments in fault zones of accretionary prisms have friction coefficients less than surrounding undeformed sediment; the collapsed fabric of the sediment in the fault zone may actually be stronger than adjacent undeformed material (Moore and Byrne, in press). Therefore, the faults may have a cyclic history of variable fluid potential. In this scenario, modeled after Sibson (1981), the fluid drains slowly into the fault zone through the low-permeability sediment; during a relatively rapid period of fault displacement, this fluid cannot be forced back into the adjacent sediment but escapes through a fracture permeability along the fault.

CONCLUSIONS

Penetration of the décollement separating the accretionary prism from the underthrusting oceanic plate, while a principal goal of our cruise, remains largely a technical achievement. The most significant scientific accomplishments of Leg 110 include:

1. Documentation of deeply derived fluids along the décollement zone and within the underthrusting sedimentary sequence. The coupled chemical and thermal anomalies along faults clearly specify active, albeit episodic, fluid flow along these conduits.
2. Discovery of fluid migration and structural fabrics developed along the level of the future décollement at the oceanic reference site. The concentrations of mud-filled veins, low-angle shear zones, and methane anomalies along the future décollement were unexpected. The seismic reflection data show no deformation related to the encroaching accretionary prism more than 3 km seaward of the deformation front.
3. Documentation of continuing deformation of the accretionary prism at Sites 673 and 674. Cores at these sites show significant structural overprints in comparison to the fabrics of cores near the deformation front. The continuing deformation occurs in sediments that are little dewatered, yet the stratal disruption, scaly mudstones, cataclastic shear zones, and deformed calcite veins combine to produce fabrics similar to those preserved in uplifted accretionary complexes.

RECOMMENDATIONS FOR FUTURE DRILLING

The success of Leg 110 in characterizing the geologic framework of the northern Barbados Ridge principally resulted from the ability of the *JOIDES Resolution* to recover core under challenging downhole conditions. Failures in logging and downhole experiments, however, limited the interpretive value of the geologic results. Our experience leads to the following recommendations that not only apply to future drilling across the northern Barbados Ridge but elsewhere in similar environments.

1. Prior to sailing, develop workable downhole instruments and a logging program to provide physical measurements to fully constrain active processes. Logging tools must be run in a manner such that the swelling clays and bridges do not interfere with their motion. A dip meter would be useful in correlating fabrics visible in cores with the regional geophysical framework.
2. Devote significant drilling effort to deeper penetrations well landward of the toe of the slope to better compare the geologic features and processes in these modern environments with those preserved in ancient rocks on land.
3. Develop reliable core orientation techniques.

ACKNOWLEDGMENTS

We acknowledge the ODP Technical and Engineering groups as well as SEDCO personnel for their contributions to the success of Leg 110. Bruce Handel assisted in analysis of the porosity data and drafted many of the figures presented here.

REFERENCES

Anderson, R. N., and Skilbeck, J. N., 1982. Oceanic heat flow. *In* Emiliani, C. (Ed.), *The Sea*, Vol. 7, *The Oceanic Lithosphere*: New York (Wiley), 489–524.

Bergen, J. A., 1984. Calcareous nannoplankton from Deep Sea Drilling Project Leg 78A: Evidence for imbricate underthrusting at the Lesser Antillian active margin: *In* Biju-Duval, B., Moore, J. C., et al, *Init. Repts. DSDP*, 78A: Washington (U.S. Govt. Printing Office), 411–445.

Biju-Duval, B., Le Quellec, P., Mascle, A., Renard, V., and Valery, P., 1982. Multibeam bathymetric survey and high resolution seismic investigations of the Barbados Ridge complex (Eastern Caribbean): A key to the knowledge and interpretation of an accretionary wedge. *In* Le Pichon, X., Augustithis, S. S., and Mascle, J., (Eds.), Geodynamics of the Hellenic Arc and Trench. *Tectonophysics*, 86:275–304.

Biju-Duval, B., Moore, J. C., et al., 1984. *Init. Repts. DSDP*, 78A: Washington (U.S. Govt. Printing Office).

Bouysse, P., 1984. The Lesser Antilles Island Arc: Structure and geodynamic evolution: in Biju-Duval, B., Moore, J. C. et al., *Init. Repts. DSDP*, 78A: Washington (U.S. Govt. Printing Office), 83–103.

Carslaw, H. S., and Jaeger, J. C., 1959. *Conduction of Heat in Solids* (2nd ed.): Oxford (Clarendon Press).

Damuth, J. E., and Fairbridge, R. W., 1970. Equatorial deep sea arkosic sands and ice-age aridity in tropical South America. *Geol. Soc. Am. Bull.*, 81:189–206.

Davis, D. M., 1984. The compressive mechanics of accretionary wedges applied to the Leg 78A study area near Barbados. *In* Biju-Duval, B., Moore, J. C. et al., *Init. Repts. DSDP*, 78A: Washington (U.S. Govt. Printing Office), 569–579.

Dorel, J., 1981. Seismicity and seismic gap in the Lesser Antilles arc and earthquake hazard in Guadeloupe: *Geophys. J. R. Astron. Soc.*, 67: 679–695.

Embley, R. W., and Langseth, M. G., 1977. Sedimentation processes on the continental rise of northeastern South America: *Mar. Geol.*, 25: 279–297.

Gieskes, J. M., 1975. Chemistry of interstitial waters of marine sediments. *Ann. Rev. Earth Planet. Sci.*, 3:433–453.

Gieskes, J. M., Johnston, K. and Boehm, M., 1984. Appendix. Interstitial water studies, Leg 66. *In* von Huene, R., Aubouin, J. et al., *Init. Repts. DSDP*, 84: Washington (U.S. Govt. Printing Office), 961–967.

Hanshaw, B. B., and Coplen, T. B., 1973. Ultrafiltration by compacted clay membrane-II Sodium ion exchange at various ionic strengths. *Geochimica et Coscmochimica Acta*, 37:2311–2327.

Karig, D. E., 1986. Physical properties and mechanical state of accreted sediments in the Nankai Trough, S. W. Japan. *In* J. C. Moore (Ed.), Structural Fabrics in DSDP Cores from Forearcs, *Geol. Soc. Am. Mem.*, 166:117–133.

Kharaka, Y. K., and Berry, F.A.F., 1973. Simultaneous flow of water and solutes through geological membranes; experimental investigation. *Geochemica et Cosmochimica Acta*, 37:2577–2603.

Ladd, J. W., Buhl, P., Bangs, N., Davis, D., and Westbrook, G., 1986. Wide-aperture seismic reflection profiling on the Barbados Ridge. *EOS*, 67:378 [Abstract].

Marlow, M. S., Lee, H., and Wright, A., 1984. Physical properties of sediment from the Lesser Antillies Margin along the Barbados Ridge: Results from Deep Sea Drilling Project Leg 78A. *In* Biju-Duval, B., Moore J. C., et al., *Init. Repts. DSDP*, 78A: Washington (U.S. Govt. Printing Office), 549–558.

Mascle, A., Biju-Duval, B., de Clarens, P., and Munsch, H., 1986. Growth of accretionary prisms: Tectonic processes from Caribbean examples. *In* Wezel, F.-C. (Ed.), *The Origin of Arcs*: Amsterdam (Elsevier), 375–400.

Maury, R. C., and Westercamp, D., 1985. Variations chronologiques et spatiales des basaltes neogene des Petites Antilles; implication sur l'evolution de l'arc. Mascle, A. (Ed.), *Symposium Geodynamique des Caraibes*: Paris (Technip) 77–90.

Molnar, P., and Sykes, L. R., 1969. Tectonics of the Caribbean and Middle America regions from focal mechanisms and seismicity. *Geol. Soc. Am. Bull.*, 80:1639–1684.

Moore, J. C., and Biju-Duval, B., 1984. Tectonic synthesis Deep Sea Drilling Project Leg 78A: Structural evolution of offscraped and

underthrust sediment, northern Barbados Ridge complex. *In* Biju-Duval, B., and Moore, J. C., et al., *Init. Repts. DSDP*, 78A: Washington (U.S. Govt. Printing Office), 601–621.

Moore, J. C., and Byrne, T., in press. Thickening of fault zones: mechanisms of melange formation in accreting sediments. *Geology.*

Ngokwey, K., 1984. Numerical modeling of sediment deformation linked to subduction: Mechanical model and comparison with Barbados Ridge Complex. *In* Biju-Duval, B., Moore, J. C. et al., *Init. Repts. DSDP*, 78A: Washington (U.S. Govt. Printing Office), 559–568.

Peter, G., and Westbrook, G. K., 1976. Tectonics of the southwestern North Atlantic and Barbados Ridge complex: *Am. Assoc. Petrol. Geol. Bull.*, 60:1078–1106.

Sibson, R. H., 1981. Fluid flow accompanying faulting: field evidence and models. *In* Simpson, D. W., and Richards, P. G. (Eds.), *Earthquake Prediction: an International Review.* Am. Geophys. Union, Maurice Ewing Series, 4:593–603.

Speed, R. C., 1983. Structure of the accretionary complex of Barbados, 1: Chalky Mount. *Geol. Soc. Am. Bull.*, 94:92–116.

Speed, R. C., Westbrook, G., Mascle, A., Biju-Duval, B., Ladd, J., Saunders, J., Stein, S., Schoonmaker, J., and Moore, J. C., 1984. Lesser Antilles Arc and adjacent terranes. *Atlas 10*, Ocean Margin Drilling Program, Regional Atlas Series: Woods Hole (Marine Science International).

Stein, S., DeMeta, C., Gordon, R., Brodholt, J., Engeln, J., Wiens, D., Argus, D., Lundgren, P., Stien, C., and Woods, D., in press. A test of alternative Caribbean Plate relative motion models.

Tomblin, J. F., 1975. The Lesser Antilles and Aves Ridge. *In* Nairn and Stelhi (Eds.), *The Ocean Basins and Margins*, 3: New York (Plenum Press), 1–64.

Torrini, R., Jr., Speed, R. C., and Mattoili, G. S., 1985. Tectonic relationships between forearc basin strata and the accretionary complex at Bath, Barbados. *Geol. Soc. Am. Bull.*, 96:861–874.

Valery, P., Nely, G., Mascle, A., Biju-Duval, B., Le Quellec, P., and Berthon, J. L., 1985, Structure et croissance d'un prisme d'accretion tectonique proche d'un continent: La ride de la Barbade au Sud de l'Arc Antillais. *In* Mascle, A., (Ed.), *Geodynamique des Caraibes*: Paris (Editions Technip), 173–186.

Waples, D. W., 1985. *Geochemistry in Petroleum Exploration*: Boston (Intl. Human Resources Development Corp).

Westbrook, G. K., Smith, M. J., Peacock, J. H., and Poulter, M. J., 1982. Extensive underthrusting of undeformed sediment beneath the accretionary complex of the Lesser Antilles subduction zone. *Nature*, 300:625–628.

Westbrook, G., Mascle, A., and Biju-Duval, B., 1984. Geophysics and structure of the Lesser Antilles forearc. *In* Biju-Duval, B., Moore, J. C., et al., *Init. Repts. DSDP*, 78A: Washington (U.S. Govt. Printing Office), 23–38.

Westercamp, D., 1977. Evolution des suies volcaniques de Martinique (FWI) et des arcs insulairs des Petites Antilles dan les contexts structural. *Transactions of the 8th Caribbean Geological Conference, Willemstad.*, 227–228.

Ms 110A-111